https://doi.org/10.5194/amt-2024-103
Preprint. Discussion started: 5 August 2024

Atmospheric Measurement Techniques Discussions

Cloud masks and cloud type classification using EarthCARE CPR and ATLID

Hajime Okamoto[1], Kaori Sato[1], Tomoaki Nishizawa[2], Yoshitaka Jin[2], Shota Ogawa[1], Hiroshi Ishimoto[3], Yuichiro Hagihara[4], Eiji Oikawa[3], Maki Kikuchi[5], Masaki Satoh[6], Woosub Roh[6].

[1]Research Institute for Applied Mechanics, Kyushu University, Fukuoka, 816-8580, Japan
[2]Earth System Division, National Institute for Environmental Studies, Tsukuba, 305-8506, Japan
[3]Meteorological Research Institute, Japan Meteorological Agency, Tsukuba, 305-0052, Japan
[4]Radio Research Institute, National Institute of Information and Communications Technology, Koganei, Tokyo, 184-8795, Japan
[5]Earth Observation Research Center, Japan Aerospace Exploration Agency, Tsukuba, Ibaraki 305-8505, Japan
[6]Atmosphere and Ocean Research Institute, The University of Tokyo, Kashiwa, Chiba 277-8564, Japan

Correspondence to: Hajime Okamoto (okamoto@riam.kyushu-u.ac.jp)

Abstract. We develop the Japan Aerospace Exploration Agency (JAXA) level 2 cloud mask and cloud type classification algorithms for the Earth Clouds, Aerosols, and Radiation Explorer (EarthCARE), a joint JAXA and European Space Agency (ESA) satellite mission. Cloud profiling radar (CPR)-only, atmospheric lidar (ATLID)-only, and combined CPR–ATLID algorithms for the cloud mask and cloud particle type are described. The algorithms are developed and evaluated using ground-based data, space-borne data from CloudSat and Cloud-Aerosol Lidar and Infrared Pathfinder Satellite Observations (CALIPSO) and simulation data from a Japanese global cloud-resolving model, the Non-hydrostatic Icosahedral Atmospheric Model (NICAM) with Joint simulator. The algorithms are based on our algorithms for CloudSat and CALIPSO with several improvements. The cloud particle type for ATLID is derived from an attenuation–depolarization diagram trained using 355 nm multiple-field-of-view multiple-scattering polarization lidar and changing the diagram from that developed for CALIPSO. The retrieved cloud particle phases (ice, water, and mixed phases) and those reported in the NICAM output data are compared. We found that the agreement for CPR-only, ATLID-only, and combined CPR–ATLID algorithms averaged roughly 80%, 85%, and 80%, respectively, for 15 different cloud scenes corresponding to two EarthCARE orbits.

1 Introduction

The greatest uncertainty in climate prediction is associated with clouds (Zelinka *et al*., 2020). Cloud phase (ice and water) information is important in climate modelling and the water/ice ratio at a given temperature varies by climate model (Tsushima *et al*., 2006), due to the uncertainty related to ice and water cloud formation mechanisms.

CALIPSO has collected cloud and aerosol information for 17 years, from its launch in 2006 by NASA and the Centre National d'Etudes Spatiales (CNES) of France until August 2023. CALIPSO lidar provides attenuated backscattering

https://doi.org/10.5194/amt-2024-103
Preprint. Discussion started: 5 August 2024


Atmospheric Measurement Techniques Discussions

coefficients at 532 and 1064 nm wavelengths and the depolarization ratio at 532 nm (Winker *et al*., 2010). The depolarization ratio has been widely used for cloud phase classification in ground-based polarization lidar observations (Sassen, 1991). Space-based and conventional ground-based lidar signals noticeably differ. The multiple scattering contributions to space-borne lidar returns increase due to the larger footprint than that of ground-based lidar for water clouds, and CALIPSO observes a greater depolarization ratio from water clouds. Vertically resolved cloud type (phase) products have been produced using CALIPSO-only data, where the cloud phase and ice particle orientation are derived based on observations of attenuation and depolarization ratio (Yoshida *et al*., 2010).

CloudSat also started observing clouds in 2006 with the first operating 94 GHz cloud radar (Stephens *et al*. 2018). The global three-dimensional distribution of clouds has been obtained using CloudSat (2B-GEOPROF products; Mace *et al*., 2007; Marchand *et al*., 2009), CALIPSO (Winker *et al*., 2007), and a combination of these two sensors (2B-GEOPROF-LIDAR products: Mace *et al*., 2009; Mace and Zhang, 2014; Kyushu University cloud mask products: Hagihara *et al*., 2010, 2014). Three-dimensional images of clouds and aerosols have increased our understanding of the atmospheric composition and radiative impact of clouds and aerosols (Stephens, 2018 and the references therein). Cloud phase identification algorithms for CloudSat and CloudSat–CALIPSO have also been developed to extend the detailed CALIPSO-based cloud type (phase) detection for clouds observed by CloudSat (Kikuchi *et al*., 2017). These cloud masks and phase products have been used extensively to evaluate global climate models (GCMs; e.g., Watanabe *et al*., 2010, 2012; Seiki *et al*., 2014) and global non-hydrostatic model results (Hashino *et al*., 2013, 2016; Roh *et al*., 2020). The cloud phase products are also used to improve Atlantic Meridional Overturning Circulation (AMOC) simulations at the Last Glacial Maximum (LGM), correcting the overestimation of ice clouds by the climate model by changing the cloud water/ice partition according to the cloud phase partition (Sherriff-Tadano *et al*., 2023) based on CALIPSO-derived phase products (Yoshida *et al*., 2010; Hirakata *et al*., 2014).

Earth Cloud, Aerosol, and Radiation Explorer (EarthCARE), a joint Japan Aerospace Exploration Agency (JAXA) and European Space Agency (ESA) satellite mission launched in May 2024, carries four sensors: 94 GHz cloud profiling radar (CPR), atmospheric lidar (ATLID), a multi-spectral imager (MSI), and a broadband radiometer (BBR). The CPR was developed by JAXA and the National Institute of Information and Communications Technology (NICT) and uses the same frequency as CloudSat and measures the Doppler velocity in the vertical direction in clouds. The sensitivity of EarthCARE CPR is –36 dBZ, which is greater than that of the CloudSat cloud profiling radar (–30 dBZ) due to the low orbit (about 400 km) of the EarthCARE satellite and large 2.5 m antenna. The 355 nm high-spectral-resolution ATLID will provide extinction and backscattering coefficients with the depolarization ratio.

Ground-based lidar with new capabilities has been developed to simulate space-borne lidar signals (Okamoto *et al*., 2016). Several attempts have also been made to extend the limitations of ground-based lidar observations using multiple scattered lidar returns, i.e., multi-field-of view (MFOV) lidar (Roy *et al*. 1999), Wide-Angle Imaging Lidar (WAIL) (Polonsky *et al*., 2005; Davis, 2008), the Cloud Thickness from Offbeam Returns (THOR) system (Cahalan *et al*. 2005). Okamoto *et al*. (2016) used the polarization capability of MFOV Multiple-Scattering Polarization Lidar (MFMSPL) in the off-beam direction for the first time, operating at 532 nm wavelength during both day and night. The first version of MFMSPL used four detectors

https://doi.org/10.5194/amt-2024-103
Preprint. Discussion started: 5 August 2024


Atmospheric Measurement Techniques Discussions

for parallel channels and four for perpendicular channels, each with a FOV of 10 mrad, to measure the depolarization ratio. The detectors were tilted at angles ranging from 0 to 30 mrad in the vertical direction at 10-mrad intervals to observe on-beam and off-beam returns. The 35-mrad half-angle FOV of MFMSPL corresponds to a receiver footprint radius of about 90 m at a height of 1 km. This is comparable to that of Cloud-Aerosol LiDAR with Orthogonal Polarization (CALIOP). The MFMSPL system was designed to simulate lidar returns similar to those observed with space-borne lidar. The 355nm-MFMSPL was further developed to simulate ATLID signals (Nishizawa *et al*., 2021). In this study, these new instruments are used to develop cloud mask and cloud particle type algorithms for EarthCARE.

In this article, we first describe the cloud mask algorithms for CPR-only, ATLID-only, and CPR or ATLID detected clouds in Section 2. The corresponding cloud particle type algorithms are also described. In Section 3, expected cloud mask and cloud type retrievals from EarthCARE are discussed using CPR and ATLID signals generated from NICAM with the Joint simulator. In Section 4, we summarize the main findings.

2 Algorithms for the JAXA Cloud mask and cloud particle type products

2-1 Cloud mask algorithms

The cloud-detection algorithms were originally developed to analyze the 94 GHz cloud radar and lidar on the research-vessel Mirai (Okamoto *et al*., 2007; Okamoto *et al*., 2008). These were also used to develop CloudSat-only, CALIPSO-only, and combined CloudSat–CALIPSO cloud-detection algorithms to produce cloud mask products from merged CloudSat and CALIPSO datasets (Hagihara *et al*., 2010, 2014). The EarthCARE CPR-only (C1), ATLID-only (C2), and combined CPR–ATLID (C4) cloud-detection algorithms are largely based on the CloudSat, CALIPSO, and combined CloudSat–CALIPSO cloud-detection algorithms (Hagihara *et al*., 2010, 2014).

The EarthCARE CPR cloud mask algorithm is an extended version of the approach applied to CloudSat and considers the two steps, i.e., (1) the threshold values for noise and (2) spatial continuity test (coherent test), to distinguish significant signals from noise and to assign a confidence level. The ATLID cloud mask is based on the attenuated backscattering coefficient in which cloudy pixels are discriminated from the grids that contain aerosols or molecules. The ATLID cloud-detection algorithm consists of a vertically varying adaptive threshold method and a spatial continuity test. The combined cloud mask products are created from the C1 and C2 mask results. The products are reported at 100 m vertical and 1 km horizontal resolutions.

2-2 Cloud particle type algorithms

2-2-1 ATLID-only cloud particle type algorithms (C2 type)

We first describe the ATLID standalone cloud particle type algorithm (C2 type), which is an extension of that for CALIPSO (Yoshida *et al*., 2010). When a single-scattering process is dominant, spherical particles in water clouds do not have a depolarization ratio (δ) although the actual measured δ usually exceeds 0%. By contrast, randomly oriented ice crystals (3D-ice) in ice clouds produce a large δ (e.g., Okamoto *et al*., 2019). Therefore, δ has been used to discriminate cloud phases using

https://doi.org/10.5194/amt-2024-103
Preprint. Discussion started: 5 August 2024


Atmospheric Measurement Techniques Discussions

ground-based polarization lidar measurements. However, satellite-borne lidar instruments such as CALIOP and ATLID observe much larger footprints (e.g., about 90 and 30 m, respectively) on the surface of the Earth than does ground-based lidar (generally less than 10 m at an altitude of 1 km). Similar discrimination is not straightforward for satellite observations because of the large δ values caused by multiple scattering in water clouds. CALIOP has a 0.13 mrad field of view (FOV, full width) and orbits Earth ~700 km above the ground, leading to a footprint size of about 90 m. ATLID has different observation conditions, e.g., a smaller FOV (0.08 mrad, full width) and orbits Earth at ~400 km, corresponding to a 26.5 m footprint. The δ of ice particles can be estimated using scattering theory, such as geometrical optics with physical optics for ice clouds (Borovoi and Kustova, 2009; Borovoi *et al*., 2012; Okamoto *et al*., 2019). From these estimates, we expect that some optically thick water clouds and ice clouds will have similar values of δ. This has been verified in the CALIPSO observations. That is, there is fundamental difficulty discriminating water from ice when we use only the measured δ value. To overcome this problem, we introduced an additional parameter for the cloud particle type, as in Yoshida *et al*. (2010) for CALIPSO. Here, we consider a similar approach for ATLID. The geometrical thickness of a layer is 100 m in ATLID. The logarithmic of the ratio of the attenuated backscattering coefficient β_{att} of layer i to that of the next layer $(i + 1)$ is estimated $[X(i) = log_{10}(\beta_{att}(i)/\beta_{att}(i+1))]$. X is known to be proportional to the transmittance of a layer when the cloud microphysics of the layers is assumed to be homogeneous.

Because theoretical estimations suggest that δ for ice particles at 355 nm is similar to that at 532 nm (Okamoto *et al*., 2020) and the X–δ relation of water clouds would differ between ATLID and CALIPSO because of the different footprint sizes, water–ice discrimination for ATLID may differ from CALIPSO for which the separation condition between ice and water was given by $\delta[\%] = 10 + 60 \cdot X^2$. To develop separation conditions for ATLID, we rely on the data obtained by the 355nm-MFMSPL (Fig. 1). In the analyses, we use only vertically pointing channels—channel 1 for the parallel direction and channel 2 for the perpendicular direction—because the channels have an FOV of 10 mrad, corresponding to about 30 m at an altitude of 3 km, which is close to the footprint size of ATLID. Observations from water cloud bottoms at altitudes < 3 km were chosen in the analyses. Using the 355nm-MFMSPL observations for 2 years, an X–δ diagram was created. The derived separation curve is $\delta[\%] = 10 + 30 \cdot X^2$. This means that a smaller δ is expected for ATLID than for CALIPSO for the same X. This new relation was incorporated into the X–δ diagram used for CALIPSO (Yoshida *et al*., 2010) to develop those applicable to ATLID, where the X–δ space assigned as water(3D-ice) is smaller(larger) than that for CALIPSO. Fig. 3 shows the resulting diagram. Note that the water cloud type for C2 clouds is first categorized by the diagram and warm or supercooled water is further categorized according to the temperature information from European Center for Medium-range Weather Forecasting (ECMWF). Spatial continuity tests (as a coherent filter) are introduced to the hydrometeor type algorithm to reduce the misclassification of cloud particle type (Yoshida *et al*., 2010). The scheme ultimately enables the creation of nine cloud particle types from ATLID: –1, missing; 0, clear; 1, warm water; 2, supercooled water; 3, 3D-ice; 4, 2D-plate; 5, a mixture of 2D-plate and 3D-ice; 6, a mixture of water and 3D ice; and 7, unknown (missing X).

https://doi.org/10.5194/amt-2024-103
Preprint. Discussion started: 5 August 2024

Atmospheric Measurement Techniques Discussions

Figure 1: Outlook of the 355nm-Multiple-Field-of-View Multiple Scattering Polarization Lidar (355nm-MFMSPL), located at NICT, Tokyo.

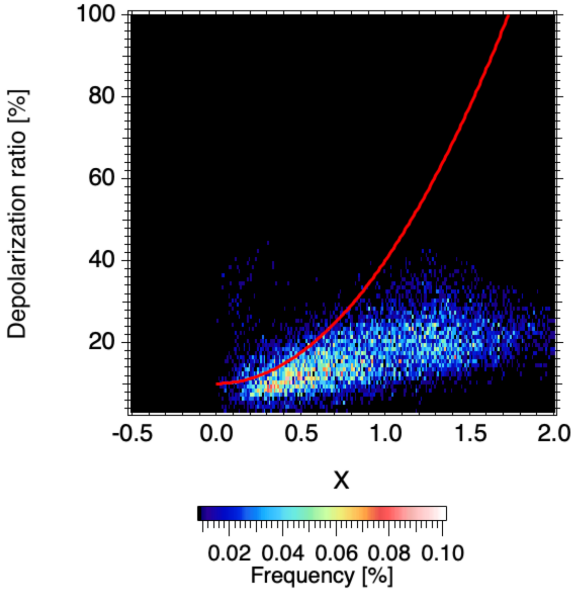

Figure 2: Depolarization ratio and *X* for water clouds at altitudes below 3 km. The data were from September 2019 to September 2021. The curve in the figure corresponds to $\delta[\%] = 10 + 30 \cdot X^2$ and separates water clouds from ice clouds.

https://doi.org/10.5194/amt-2024-103
Preprint. Discussion started: 5 August 2024

Atmospheric Measurement Techniques Discussions

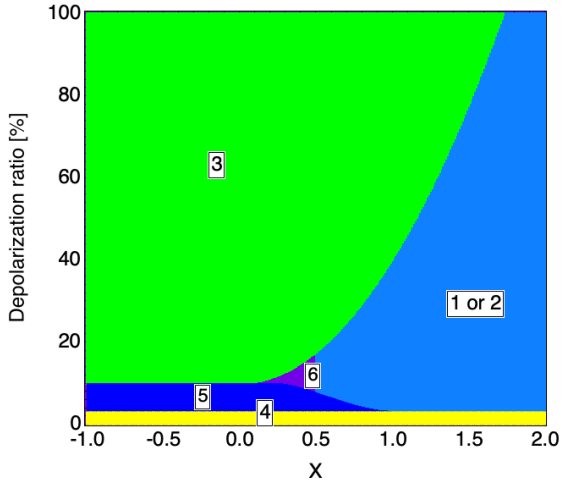

Figure 3: X–δ diagram for discriminating cloud particle type for ATLID. The numbers in the figure correspond to the following cloud particle types: 1, warm water; 2, supercooled water; 3, 3D-ice; 4, 2D-plate; 5, a mixture of 2D-plate and 3D-ice; and 6, a mixture of water and 3D ice.

2-2-2 CPR-only cloud particle type algorithm (C1 type)

The cloud particle type for C1 clouds is determined using CPR alone (C1-type) to infer cloud phase, ice orientation and precipitation type (Kikuchi *et al*. 2017). Radar Ze data from CPR and temperature data from ECMWF are used for initial hydrometeor type classification and precipitation correction and spatial continuity schemes are introduced to reduce the misclassification of cloud particle type in the CPR-only cloud particle type algorithm. Further, a Ze and temperature-based melting layer detection scheme is developed and implemented in the hydrometeor type classification scheme to determine the ice–water mixing layers. CPR has 11 cloud particle types: –9, missing; 0, clear; 1, warm water; 2, supercooled water; 3, 3D-ice; 4, 2D-plate; 5, liquid drizzle; 6, mixed phase drizzle; 7, rain; 8, snow and; 9, melting layer. The melting layer (ML) can be characterized as dark band near 0°C where snow particles start melting (Kollias and Albrecht 2005). ML top altitude is identified by local minimum of Ze in the profile and the bottom altitude of the ML is determined by the end of sharp increase of Ze toward the bottom. These features are detected from the weighting averaged value of the vertical derivative of Ze calculated using surrounding pixels to improve ML detection. Fig. 4 shows the results of the C1 type based on CloudSat with the retrieved C1-type shown in the Ze-temperature diagram.

https://doi.org/10.5194/amt-2024-103
Preprint. Discussion started: 5 August 2024

Atmospheric Measurement Techniques Discussions

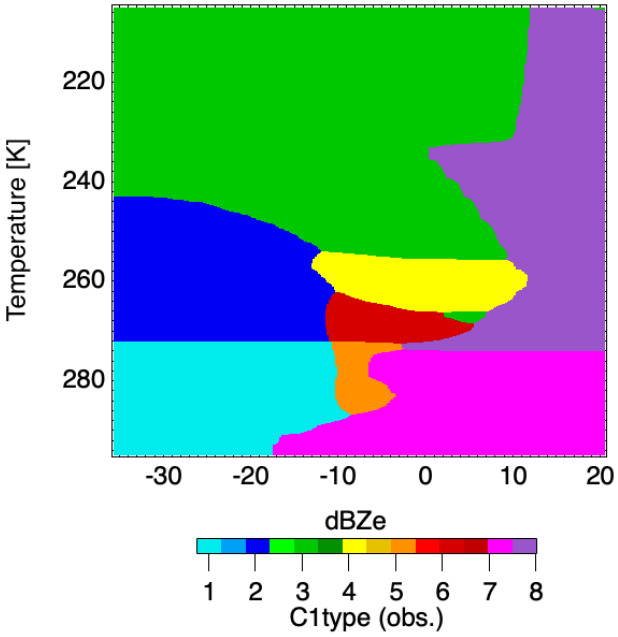

Figure 4: Retrieved results of the C1 particle type from CloudSat data. The numbers in the figure correspond to the particle type: 1, warm water; 2, supercooled water; 3, 3D-ice; 4, 2D-plate; 5, liquid drizzle; 6, mixed phase drizzle; 7, rain; and 8, snow. Here melting layer is not included.

2-2-3 Algorithms for the combined CPR–ATLID cloud particle type (C4 type)

The CPR- and ATLID-type classification schemes are combined as the CPR–ATLID classification scheme (C4 type), which is applicable to CPR or ATLID detected cloud regions. The C4 type scheme uses information on the particle types from the C1- and C2-type schemes for each observation grid to reclassify the particle type similar to the CloudSat and CALIPSO type (Kikuchi *et al*., 2016). Consequently, the following 16 hydrometeor types are obtained from the C4 type scheme: -9, missing; 0, clear; 1, warm water; 2, supercooled water; 3, 3D-ice; 4, 2D-plate; 5, mixture of 3D-ice and 2D-plate; 6, liquid drizzle; 7, mixed-phase drizzle; 8, rain; 9, snow; 10, water and liquid drizzle; 11, water and rain; 12, mixed phase; 13, unknown; and 14, melting layer. If the particle type is 7 or 12, the cloud particle phase is categorized as mixed phase.

In the next section, the EarthCARE algorithms for cloud mask and cloud particle type are applied to simulated EarthCARE L1 data for CPR and ATLID from the NICAM/Joint simulator and the retrieval performance is assessed.

3. Demonstration of the retrieval results and evaluations

The JAXA L1 data for all four sensors onboard EarthCARE are simulated by using the output from NICAM (Tomita and Satoh, 2004; Satoh *et al*., 2008; Satoh *et al*., 2010, 2014) and a forward simulator called the Joint simulator (Hashino *et al*., 2013, 2016; Satoh *et al*., 2016). The cloud and precipitation properties were simulated with a bulk single-moment cloud

https://doi.org/10.5194/amt-2024-103
Preprint. Discussion started: 5 August 2024


Atmospheric Measurement Techniques Discussions

microphysics scheme with six water categories (NSW6; Tomita 2008). Global 3D aerosols (sulfate, soil dust, sea salt, black carbon, and organic matter) and their radiative properties were simulated using the NICAM Spectral Radiation-Transport Model (NICAM-SPRINTARS) (Takemura *et al*. 2000). For the Joint simulator, the basic structure follows the NASA Goddard SDSU (Masunaga *et al*., 2010). CPR and ATLID signals are calculated by the EarthCARE Active sensor simulator (EASE) implemented in the Joint simulator (Okamoto *et al*., 2007, 2008; Nishizawa *et al*., 2008). Details are described in Roh *et al*. (2023). We chose three scenes for detailed analyses and used 15 different cloud scenes corresponding to data from about two full EarthCARE orbits to evaluate the accuracy of the algorithms.

3-1 Mid-latitude scene

This scene contains geometrically thick clouds and precipitation. The cloud top height is around 12 km. Fig. 5 shows a time–height cross-section of Ze from CPR (Fig. 5a), the cloud backscattering coefficient (Fig. 5b), and the cloud depolarization ratio (Fig. 5c). The last two are from the ATLID L2a product processed by the National Institute for Environmental Studies (Nishizawa *et al*., 2024) after applying the ATLID cloud mask. We applied the cloud mask and cloud particle type algorithms to these simulated CPR and ATLID signals. For this scene, the cloud areas detected with C1 and C4 are similar. This means that only a small improvement is achieved by adding the C2 mask for ATLID to the C1 mask to create the C4 mask results. Fig. 6 shows the results for the retrieved cloud particle types using the C1, C2, and C4 type algorithms. The scene contained ice particles above 2–4 km and rain below 2–4 km. The retrieved C2 type contained 3D-ice and warm water but almost no 2D-plate in the scene.

https://doi.org/10.5194/amt-2024-103
Preprint. Discussion started: 5 August 2024

Atmospheric Measurement Techniques Discussions

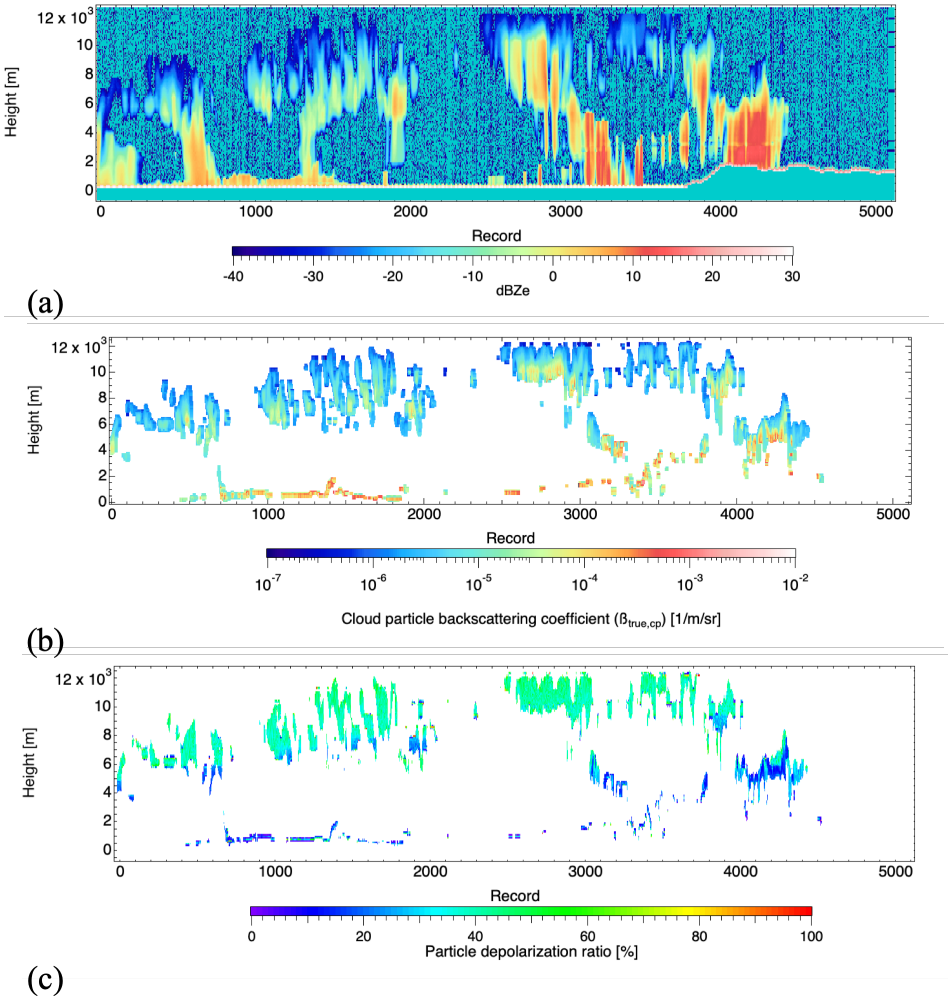

Figure 5: CPR and ATLID simulated by the NICAM-Joint simulator for the mid-latitude case on June 19 2008. (a) Time height cross-section of the simulated radar reflectivity factor (Ze) from CPR. (b) The same as (a), but for the cloud particle backscattering coefficient derived from ATLID L1 data simulated using the ATLID L2a algorithms. (c) The same as (a), but for the cloud particle depolarization ratio simulated from ATLID L2a algorithms.

https://doi.org/10.5194/amt-2024-103
Preprint. Discussion started: 5 August 2024

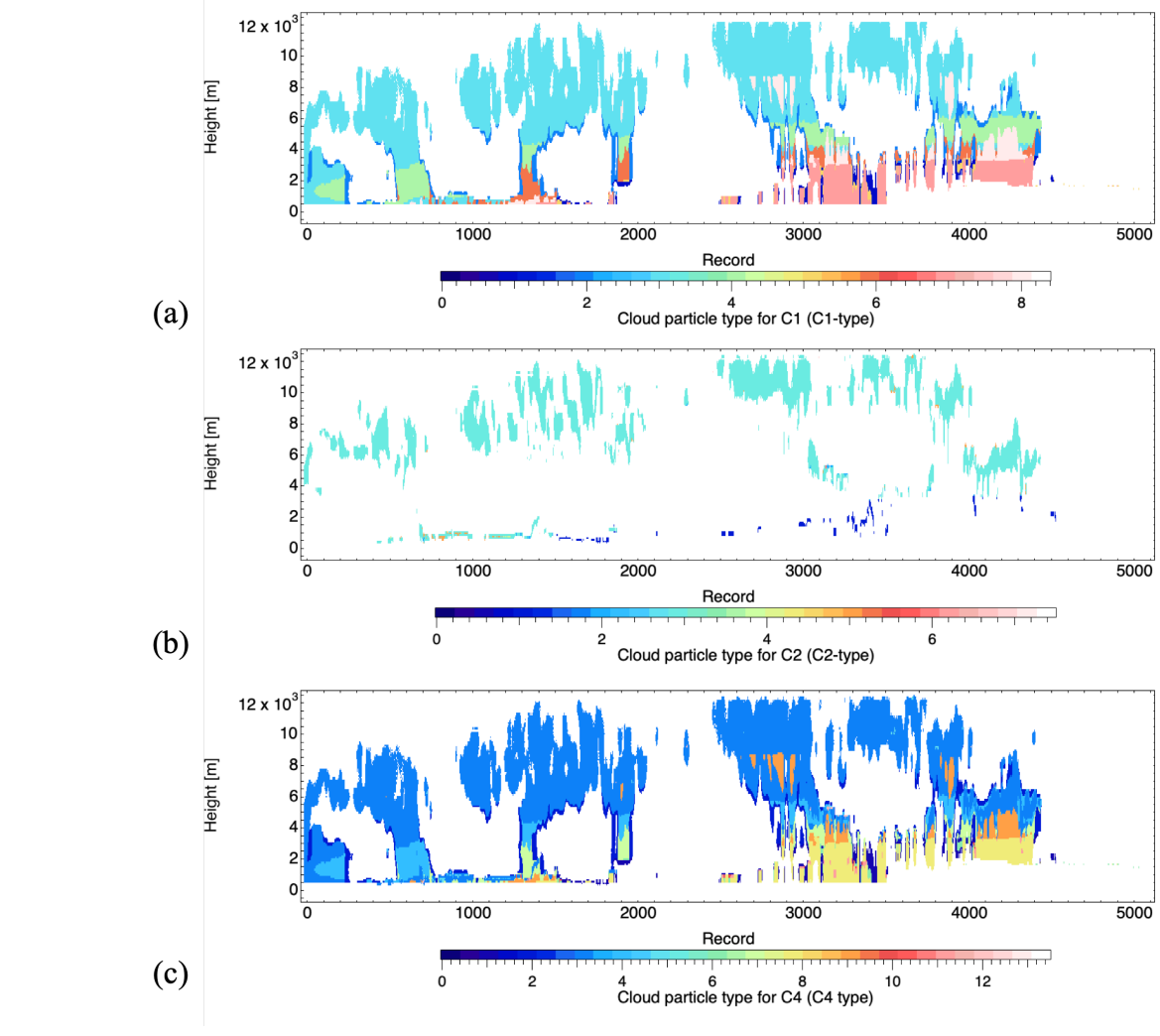

225

Figure 6: Retrieved cloud particle types: (a) C1, (b) C2, and (c) C4 types.

For evaluation purposes, the retrieved C4 cloud types are further grouped into water (1, 2, 6, 8, 10, 11), ice (3, 4, 5 ,9), and mixed (7, 12, 14) phases. These retrieved phases are compared with the phase information from NICAM. Note that ice and water particles can co-exist in the same NICAM grid, so that the mixed phase can be also compared. Fig. 7 compares the retrieved and original cloud particle phase outputs. Phases 1, 2, and 3 denote the water, ice, and mixed phases, respectively. There is overall agreement in the comparisons, although discrepancies are also found. The mixed phase was overestimated in the first half of the records and underestimated in the second half. The agreement between the C2 type and NICAM is slightly better than for the C1 type.

https://doi.org/10.5194/amt-2024-103
Preprint. Discussion started: 5 August 2024

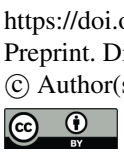

Atmospheric Measurement Techniques Discussions

Agreement rates were estimated for the retrieved C1, C2, and C4 types as follows. When the phase type (1, 2, or 3) of the grid of interest agrees with the phase type from NICAM, the type for the grid is considered to be in agreement. When the C4 phase is 1 (water) and the NICAM phase for the C4 phase is 3 (mixed phase), the grid disagrees. The total numbers of C1 (N_{tot}(C1)), C2 N_{tot}(C2)). and C4 (N_{tot}(C4)) phase types were 205961, 61810, and 206788, respectively in this scene. Then, the numbers of grids in agreement for C1, C2, and C3, [$N_{tot,a}$(C1), $N_{tot,a}$(C2), and $N_{tot,a}$(C4)], are counted and the agreement ratio is determined as $N_{tot,a}$(Ci)/N_{tot}(Ci) for i=1–3. The agreement rate for C1, C2, and C4 types was 78.7%, 83.5% and 78.4%, respectively.

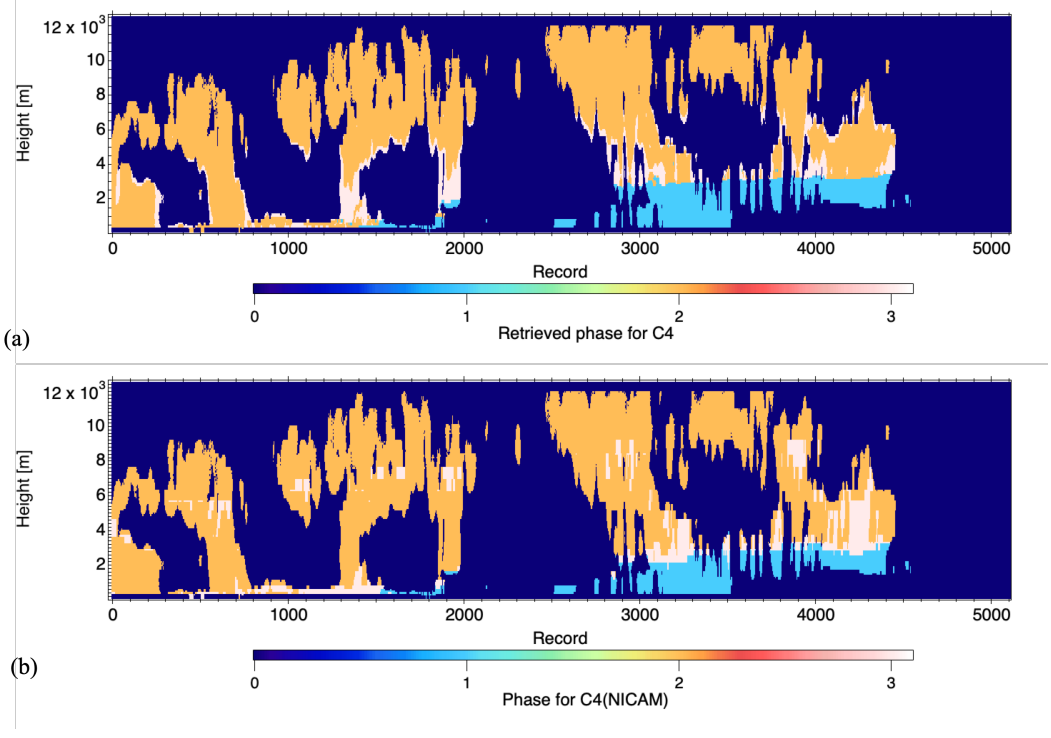

Figure 7: (a) Retrieved cloud particle phase for C4 and (b) the original phase in NICAM.

3-2 Tropics scene

This scene contains high cirrus clouds located at 15–16 km altitudes and was partly associated with precipitation in the Tropics. The Ze of high cirrus clouds is often very small, i.e., close to –35 dBZe (Fig. 8). Convection can be observed fully by CPR for around 3500 records, while ATLID signals were attenuated below 15 km. The retrieved C4 types were 3D-ice at upper altitudes (>10 km) and rain below 5 km. Overall agreement for the phase was found (Fig. 9). In this scene, N_{tot}(C1), N_{tot}(C2), and N_{tot}(C4) were 77939, 30860, and 80581, respectively. The agreement rates are very high for C1, C2, and C4, at 92.4%, 95.8%,

https://doi.org/10.5194/amt-2024-103
Preprint. Discussion started: 5 August 2024

Atmospheric Measurement Techniques Discussions

and 92.5%, respectively.

255

(a)

(b)

(c)

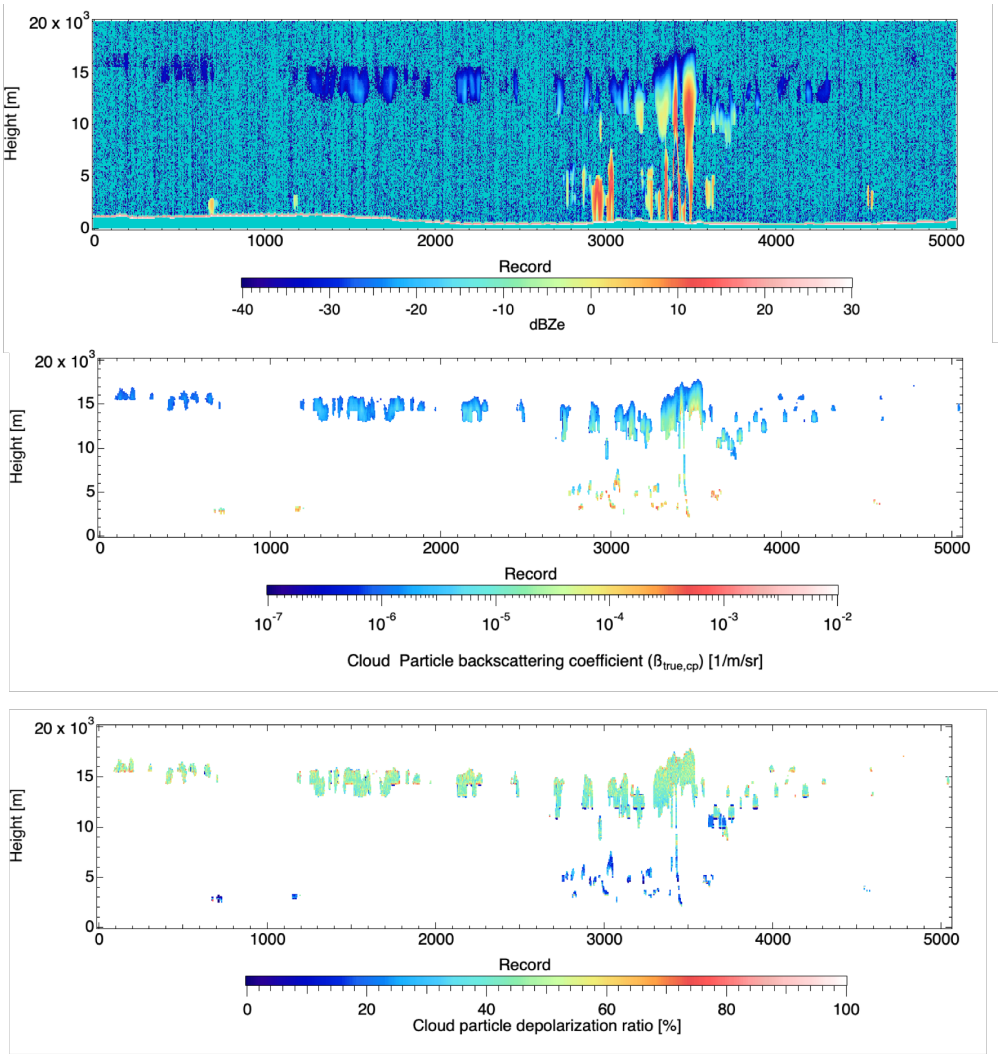

Figure 8: The same as Figure 5 but for the Tropics.

260

https://doi.org/10.5194/amt-2024-103
Preprint. Discussion started: 5 August 2024

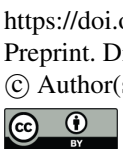

Atmospheric Measurement Techniques Discussions

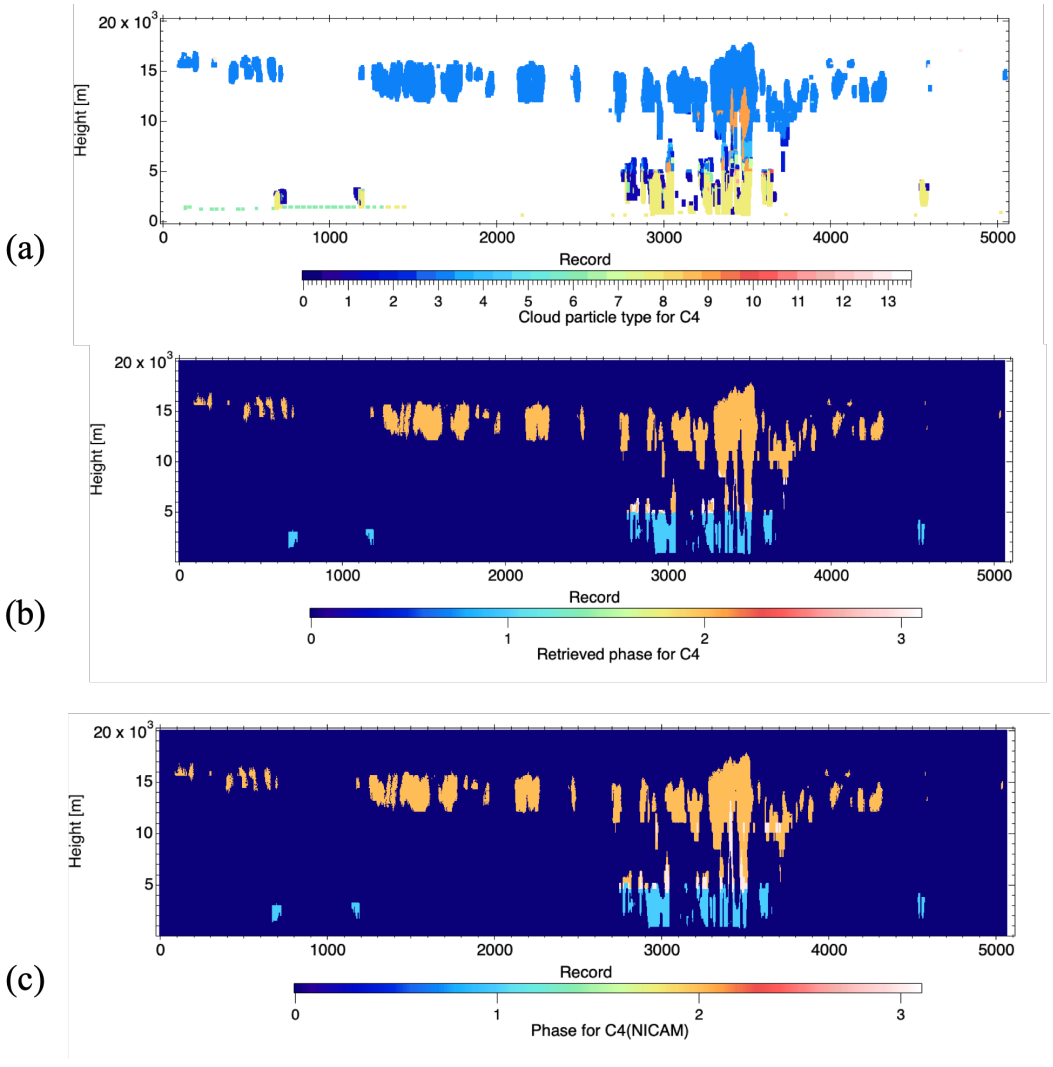

Figure 9: (a) Retrieved cloud particle type for C4; (b) retrieved phase for C4; and (c) the original phase in NICAM for the Tropics.

3-3 Antarctic scene

Clouds and snow scenes in Antarctica were chosen to demonstrate the cloud particle type (Fig. 10). Strong CPR echoes >10 dBZe were found in records between 1300 and 1800. The retrieved cloud particle type for C4 is mostly 3D-ice, with some snow corresponding to the strong dBZe . Comparing the retrieved phases with those from NICAM, the agreement rates were very high for C1, C2, and C4 at 92.0%, 88.6%, and 92.0%, respectively (Fig. 11).

https://doi.org/10.5194/amt-2024-103
Preprint. Discussion started: 5 August 2024

Atmospheric Measurement Techniques Discussions

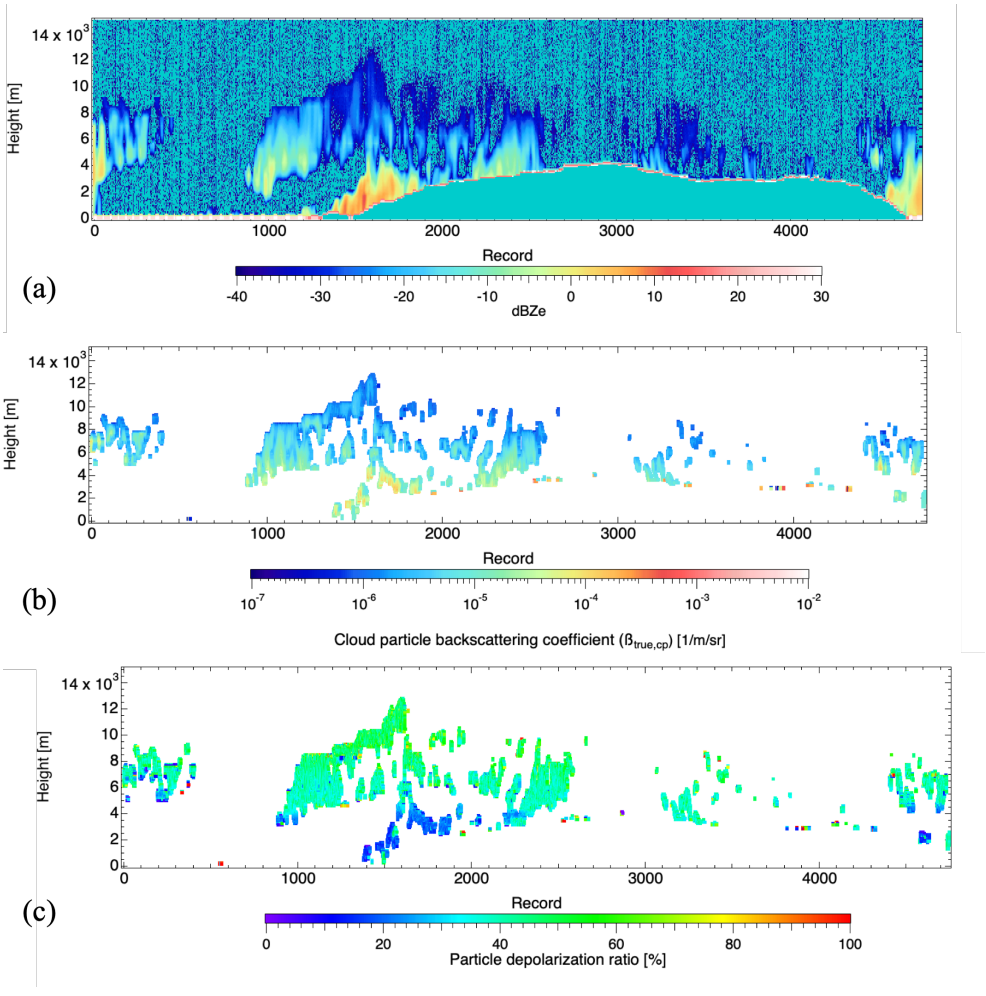

Figure 10: The same as Figure 5 but for Antarctica.

https://doi.org/10.5194/amt-2024-103
Preprint. Discussion started: 5 August 2024

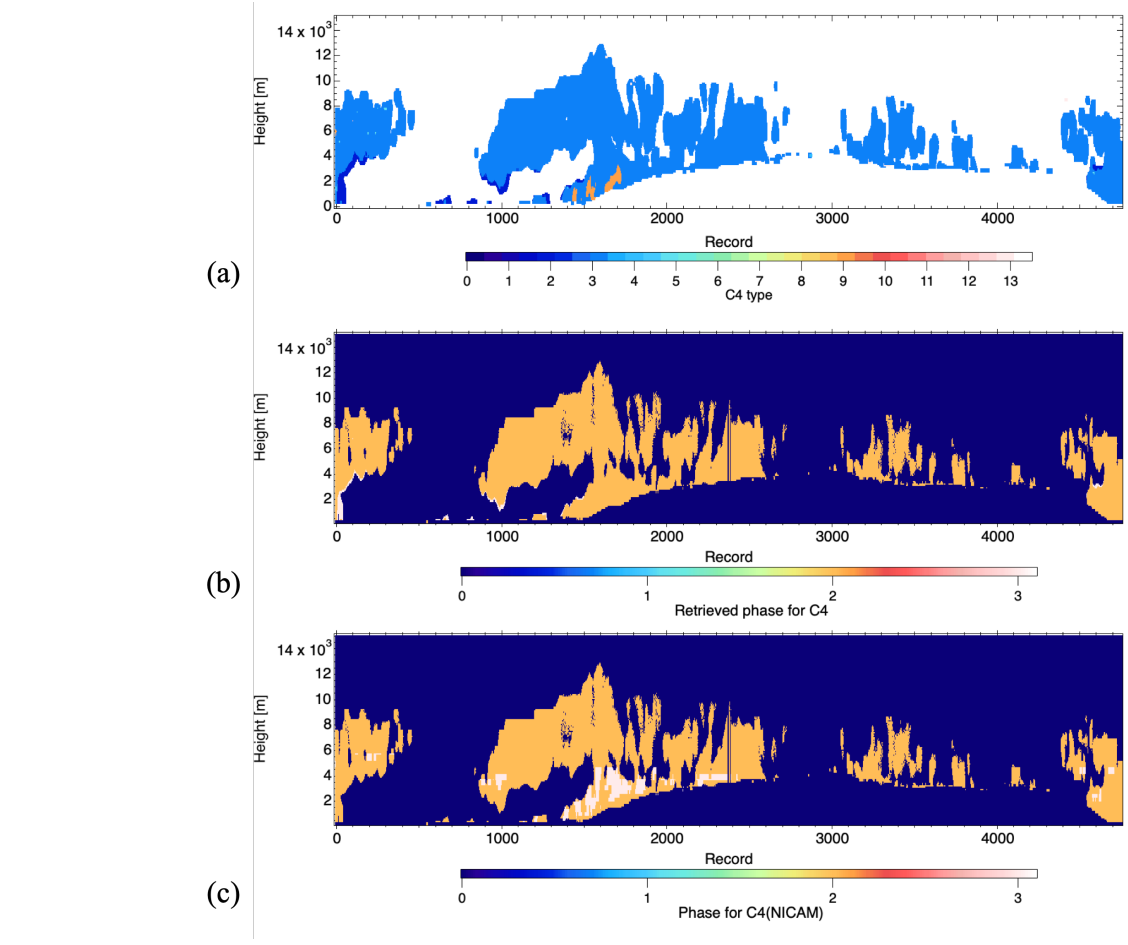

Figure 11: (a) Retrieved cloud particle type for C4; (b) retrieved phase for C4; and (c) the original phase in NICAM for the Antarctica.

3-4 Evaluation of the phase classification using simulated EarthCARE L1 data for full orbits

We examined the mean agreement rate for phase using total 15 simulated scenes (two full Earth orbits). In the scenes, N_{tot}(C1), N_{tot}(C2), and N_{tot}(C4) were 1790520, 514498, and 1807070, respectively. The agreement rates for C1, C2, and C4 were 80.3%, 85.3%, and 80.0%, respectively.

4 Summary

This article describes the JAXA level 2 (L2) cloud mask and cloud particle type algorithms for CPR and ATLID onboard the EarthCARE satellite. The EarthCARE L2 cloud mask algorithms for C1, C2, and C4 are similar to those for CloudSat and CALIPSO. To develop the cloud particle type for ATLID, we used multiple scattering polarization lidar (355nm-MFMSPL). The depolarization–attenuation diagram for ATLID was newly developed using water cloud data for 2 years obtained by the

https://doi.org/10.5194/amt-2024-103
Preprint. Discussion started: 5 August 2024


Atmospheric Measurement Techniques Discussions

355nm-MFMSPL with theoretical estimates of ice particles. For the C1 type for CPR, the algorithm developed for CloudSat was extended using the Ze and temperature relation to classify cloud particle types. The CPR- and ATLID- type classification schemes are combined as the CPR–ATLID classification scheme.

The developed algorithms were evaluated using NICAM-Joint simulator EarthCARE L1 signals and by comparing the retrieved cloud particle phase and original outputs from NICAM. Detailed analyses are shown for mid-latitudes, the Tropics, and Antarctica. The agreement rates of the retrieved cloud phases were equal or better than 80% for C1, C2, and C4. The C2 type generally agreed better with NICAM than the C1 type.

Several possible extensions of the algorithms are possible. Doppler velocity (Vd) information from CPR can help discriminate the phase for precipitation and Vd is incorporated into the C1 and C4 type algorithms for JAXA L2 research products. Extinction can be obtained directly by ATLID. Instead of using the ratio of two vertically successive backscattering coefficients, a depolarization ratio–extinction diagram might be realized for some cloud regions with sufficient signal-to-noise ratios for extinction. These extensions of the algorithms will give more accurate particle phase information.

Once the cloud mask and type are retrieved, they can be used to derive cloud particle categories (Sato and Okamoto, 2023) and cloud microphysics using the CPR, ATLID, and CPR–ATLID algorithms (Sato *et al*., 2024). It is also necessary to evaluate the algorithms using actual observed data. We have developed a comprehensive ground-based observation system that consists of ground-based active sensors: 94GHa High-sensitivity Ground-based Super Polarimetric Ice-crystal Detection and Explication Radar (HG-SPIDER); 355nm-Multiple-Field-of-view Multi Scattering Polarization lidar (Okamoto et al,, 2016; Nishizawa *et al*., 2020); 355nm-high-spectral resolution lidar with polarization (Jin *et al*., 2021); 355nm-Doppler lidar (Ishii *et al*., 2022); and 2 μm-Doppler lidar (Iwai *et al*., 2013) operated at the NICT Koganei site in Tokyo, Japan. Other datasets will be used to evaluate the EarthCARE L2 cloud and precipitation products, including a wind profiler network operated by Japan Meteorological Agency in Japan and K-band radar with disdrometer observations in Antarctica (Bracci *et al*., 2023).

Data availability.

The JAXA EarthCARE synthetic data is distributed from https://doi.org/10.5281/zenodo.7835229 (Roh et al., 2023). The JAXA L2 Echo products and ATLID products were processed by the National Institute of Information and Communications Technology (PI: Horie H.) and National Institute for Environmental Studies (PI: Nishizawa, T.), respectively. CPR, CPR-ATLID and CPR-ATLID-MSI cloud products were processed by Kyushu University (PI: Okamoto, H. O.). The CALIPSO Lidar Level 1B profile data and CloudSat 2B-GEOPROF data used in this study are provided from the NASA Langley Research Center Atmospheric Science Data Center (https://doi.org/10.5067/CALIOP/CALIPSO/LID_L2_05KMCLAY-STANDARD-V4-20) and CloudSat Data Processing Center (https://www.cloudsat.cira.colostate.edu/data-products/2b-geoprof, Marchand & Mace, 2018), respectively. The KU CloudSat-CALIPSO merged data sets and cloud products and CALIPSO aerosol products, are provided and updated to the latest version by JAXA EarthCARE Research A-Train Product Monitor (https://www.eorc.jaxa.jp/EARTHCARE/research_product/ecare_monitor_e.html).

Author contributions.

https://doi.org/10.5194/amt-2024-103
Preprint. Discussion started: 5 August 2024

HO coordinated the work and drafted the paper. KS edited the text. HO, YH, EO and KS developed JAXA L2 cloud mask algorithm for CPR. HO, TN, YJ developed the cloud mask for ATLID. TN, YJ and HO developed the 355nm-MFMSPL. HO and SO developed ATLID cloud particle type algorithm. HO, KS and MK developed CPR and CPR-ATLID cloud particle type algorithms. HI conducted the lidar backscattering calculations for ice particles. KS integrated the algorithms. MS and WR developed the EarthCARE synthetic data and provided the NICAM model outputs.

Competing interests.

The authors have no competing interests to declare.

Special issue statement.

This article is part of the special issue "EarthCARE Level 2 algorithms and data products." It is not associated with a conference.

Acknowledgements.

The authors would like to thank the JAXA EarthCARE Science Team and the Remote Sensing Technology Center of Japan (RESTEC).

Financial support.

This study was supported by The Japan Aerospace Exploration Agency for the EarthCARE mission (grant no. 24RT000246; 24RT000193); JSPS (KAKENHI Grants JP24H00275; JP22K03721); Research Institute for Applied Mechanics, Kyushu University (Fukuoka, Japan).

References

Borovoi, A., Konoshonkin, A., Kustova, N., and H. Okamoto, H.:Backscattering Mueller matrix for quasi-horizontally oriented ice plates of cirrus clouds: application to CALIPSO signals," Opt. Express **20**(27), 28222–28233, 2012.

Bracci, A., Sato, K., Baldini, L., Porcù, F., and Okamoto, H.: Development of a methodology for evaluating spaceborne W-band Doppler radar by combined use of Micro Rain Radar and a disdrometer in Antarctica, Remote Sensing of Environment, 294, 113630, https://doi.org/10.1016/j.rse.2023.113630, 2023.

Cesana, G., and Chepfer, H.: Evaluation of the cloud ther- modynamic phase in a climate model using CALIPSO- GOCCP. J. Geophys. Res. Atmos., 118, 7922–7937, https:// doi.org/10.1002/jgrd.50376, 2013.

Cesana, G., et al., Using in situ airborne measurements to evaluate three cloud phase products derived from CALIPSO, J. Geophys. Res. Atmos., 121, 5788–5808, doi:10.1002/ 2015JD024334, 2016.

https://doi.org/10.5194/amt-2024-103
Preprint. Discussion started: 5 August 2024

Davis, A. B: Multiple-scattering lidar from both sides of the clouds: Addressing internal structure, J. Geophys. Res. 113(D14), D14S10, 2008.

Caharan, R. F., McGill, M. and Kolansinski, J.: THOR-cloud thickness from offbeam lidar returns,J. Atmos. Ocean. Technol. 22(6), 605–627, 2005.

Hagihara, Y., Okamoto H., and Yoshida,R.: Development of a combined CloudSat/CALIPSO cloud mask to show global cloud distribution, J. Geophys. Res., doi:10.1029/2009JD012344, 115, D00H33, 2010.

Hagihara, Y., Okamoto, H. and Luo, Z. J.: Joint analysis of cloud top heights from CloudSat and CALIPSO: New insights into cloud top microphysics, J. Geophys. Res. Atmos., 119, 4087-4106, doi:10.1002/2013JD020919, 2014.

Hashino, T., Satoh M., Hagihara, Y., Kubota,T., Matsui T., Nasuno T., and Okamoto H.: Evaluating cloud microphysics from NICAM against CloudSat and CALIPSO, J. Geophys. Res. Atmos., 118, 7273–7292, doi:10.1002/jgrd.50564, 2013.

Hashino, T., Satoh, M., Hagihara, Y., Kato, S., Kubota, T., Matsui, T., and Sekiguchi, M.: Evaluating Arctic cloud radiative effects simulated by NICAM with A-train, J. Geophys. Res.-Atmos., 121, 7041−7063, 2016.

Hirakata, M., H. Okamoto, Y. Hagihara, T. Hayasaka, and R. Oki: Comparison of global and seasonal characteristics of cloud phase and horizontal ice plates derived from CALIPSO with MODIS and ECMWF. J. Atmos. Oceanic Technol., 31, 2114–2130, https://doi.org/10.1175/JTECH-D-13-00245.1, 2014.

Hu, Y., Winker, D., Vaughan, M., Lin, B., Omar, A., Trepte, C., Flitter, D., Yang, P., NASIRI, S. Baum, B., Sun, W., Liu,Z., Wang, Z., Young, S., Stamnes, K., Huang J., Kuehn, R. and Holz R., CALIPSO/CALIOP Cloud Phase Discrimination Algorithm 2293-2309, DOI: 10.1175/2009JTECHA1280.1, JTECH, 2009.

Ishii, S., Kishibuchi, K., Takenaka, H., Jin, Y., Nishizawa, T., Sugimoto, N., Iwai, H., Aoki, M., Kawamura, S., and Okamoto, H.: 355-nm direct-detection Doppler wind lidar for vertical atmospheric motion measurement, Appl. Opt., 61, 7925, https://doi.org/10.1364/ao.460219, 2022.

Iwai, H., Ishii, S. ., Oda, R., Mizutani, K., Sekizuka, S. and Murayama, Y.: Performance and Technique of Coherent 2-mm Differential Absorption and Wind Lidar for Wind Measurement, Journal of Atmospheric and Oceanic Technology, 30(3), 429-449, doi:10.1175/JTECH-D-12-00111.1, 2013.

Jin, Y., Nishizawa, T., Sugimoto, N., Ishii, S., Aoki, M., Sato, K., and Okamoto, H.: Development of a 355-nm high-spectral-resolution lidar using a scanning Michelson interferometer for aerosol profile measurement, Opt. Express, 28, 23209, https://doi.org/10.1364/oe.390987, 2020.

Kikuchi, M., Okamoto, H., Sato, K., Suzuki, K., Cesana G., Hagihara, Y., Takahashi, N., Hayasaka, T., Oki, R.: Development of algorithm for discriminating hydrometeor particle types with a synergistic Use of CloudSat and CALIPSO. Journal of Geophysical Research: Atmospheres, 122, 11,022–11,044. https://doi.org/10.1002/ 2017JD027113, 2017.

https://doi.org/10.5194/amt-2024-103
Preprint. Discussion started: 5 August 2024

Atmospheric Measurement Techniques Discussions

Kollias, P., and Albrecht, B.: Why the melting layer radar reflectivity is not bright at 94GHz. Geophysical Research Letters, 32, L24818, https://doi.org/10.1029/2005GL024074, 2005.

Mace, G. G., Marchand, R., Zhang, Q., and Stephens, G. L.: Global hydrometeor occurrence as observed by CloudSat: Initial observations from summer 2006, Geophys. Res. Lett., 34, L09808, doi:10.1029/ 2006GL029017, 2006.

Mace, G. G., Q. Zhang, M. Vaughan, R. Marchand, G. Stephens, C. Trepte, and D. Winker, D:,A description of hydrometeor layer occurrence statistics derived from the first year of merged Cloudsat and CALIPSO data, J. Geophys. Res., 114, D00A26, doi:10.1029/2007JD009755, 2009.

Mace, G. G., and Q. Zhang, Q.: The CloudSat radar-lidar geometrical profile product (RL-GeoProf): Updates, improvements, and selected results, J. Geophys. Res. Atmos., 119, 9441–9462, doi:10.1002/2013JD021374, 2014.

Marchand, R. T., Mace, G. G., and Ackerman, T. P.: Hydrometeor detection using CloudSat: An Earth orbiting 94 GHz cloud radar, J. Atmos. Oceanic Technol., 25, 519–533, doi:10.1175/2007JTECHA1006.1, 2008.

Masunaga, H., Matsui, T., Tao, W. K., Hou, A. Y., Kummerow, C. D., Nakajima, T., Bauer, P., Olson, W. S., and Sekiguchi, M., and Nakajima, T. Y.: Satellite data simulator unit: a multisensor, multispectral satellite simulator package, B. Am. Meteorol. Soc., 91, 1625−1632, https://doi.org/10.1175/2010BAMS2809.1, 2010.

Nishizawa, T., Jin, Y., Sugimoto, N., Sato, K., Fujikawa, M., Ishii, S., Aoki, M., Nakagawa, K., and Okamoto, H.: Observation of clouds, aerosols, and precipitation by multiple-field-of-view multiple-scattering polarization lidar at 355 nm, Journal of Quantitative Spectroscopy and Radiative Transfer, 271, 107710, https://doi.org/10.1016/j.jqsrt.2021.107710, 2021.

Okamoto, H., Nishizawa,T., Takemura,T., Kumagai, K., Kuroiwa, H., Sugimoto, N., Matsui, I., Shimizu, A., Kamei, A., Emori, S. and Nakajima, T.: Vertical cloud structure observed from shipborne radar and lidar, : mid-latitude case study during the MR01/K02 cruise of the R/V Mirai, J. Geophys. Res, 112, D08216, doi:10.1029/2006JD007628, 2007.

Okamoto, H., Nishizawa, T., Takemura, T., Sato, K., Kumagai, H. Ohno, Y., Sugimoto, N., Matsui, I., Shimizu, A. and Nakajima, T.: Vertical cloud properties in Tropical Western Pacific Ocean: Validation of CCSR/NIES/FRCGC GCM by ship-borne radar and lidar, J. Geophys. Res., 113, D24213, doi:10.1029/2008JD009812, 2008

Okamoto, H., Sato, K., Nishizawa, T., Sugimoto, N., Makino, T., Jin, Y., Shimizu, A., Takano, T., and Fujikawa, M.: Development of a multiple-field-of-view multiple-scattering polarization lidar: comparison with cloud radar, Opt. Express, 24, 30053, https://doi.org/10.1364/oe.24.030053, 2016.

Okamoto, H., Sato, K., Borovoi, A., Ishimoto, H., Masuda, K., Konoshonkin, A., and Kustova, N.: Interpretation of lidar ratio and depolarization ratio of ice clouds using spaceborne high-spectral-resolution polarization lidar, Opt. Express, 27, 36587, https://doi.org/10.1364/oe.27.036587, 2019.

Okamoto, H., Sato, K., Borovoi, A., Ishimoto, H., Masuda, K., Konoshonkin, A., and Kustova, N.: Wavelength dependence of ice cloud backscatter properties for space-borne polarization lidar applications, Opt. Express, 28, 29178, https://doi.org/10.1364/oe.400510, 2020.

Okamoto, H,, Sato K, Nishizawa T., Jin Y., Ishimoto H, Oikawa E., Hagihara Y., Ogawa S., Cloud mask and particle type classification using EarthCARE CPR and ATLID, Atmos. Meas. Tech., submitted, 2024.

Polonsky, N.I., S. P. Love, S. P. and Davis, A. B.: Wide-Angle Imaging Lidar development at the ARM Southern Great Plains site: Intercomparison of cloud property retrievals, J. Atmos. Ocean. Technol. 22(6), 628–648, 2005.

Roh,W., Satoh, M., Hashino, T., Okamoto, H., Seiki, T.: Evaluations of the Thermodynamic Phases of Clouds in a Cloud-System-Resolving Model Using CALIPSO and a Satellite Simulator over the Southern Ocean, J. Atmos. Sci, 10.1175/JAS-D-19-0273.1, **77**, 11, (3781-3801), 2020.

Roh, W., Satoh, M., Hashino, T., Matsugishi, S., Nasuno, T., and Kubota, T.: Introduction to EarthCARE synthetic data using a global storm-resolving simulation, Atmos. Meas. Tech., 16, 3331–3344, https://doi.org/10.5194/amt-16-3331-2023, 2023.

Roy, G., Bissonnette, L., Bastille, C., and Vallée, G.: Retrieval of droplet-size density distribution from multiple-field-of-view cross-polarized lidar signals: theory and experimental validation, Appl. Opt. 38(24), 5202–5211, 1999.

Sassen, K.: The polarization lidar technique for cloud research: A review and current assessment," Bull. Am. Meteorol. Soc. 72(12), 1848–1866, DOI: https://doi.org/10.1175/1520-0477(1991)072<1848:TPLTFC>2.0.CO;2, 1991.

Satoh, M., Matsuno, T., Tomita, H., Miura, H., Nasuno, T., and Iga, S.: Nonhydrostatic icosahedral atmospheric model (NICAM) for global cloud resolving simulations, J. Comput. Phys., 227, 3486– 3514, https://doi.org/10.1016/j.jcp.2007.02.006, 2008.

Satoh, M., Inoue, T., and Miura, H.: Evaluations of cloud properties of global and local cloud system resolving models using CALIPSO and CloudSat simulators, J. Geophys. Res., 115, D00H14, https://doi.org/10.1029/2009JD012247, 2010.

Satoh, M., Tomita, H., Yashiro, H. *et al.* : The Non-hydrostatic Icosahedral Atmospheric Model: description and development. *Prog. in Earth and Planet. Sci.* **1**, 18. https://doi.org/10.1186/s40645-014-0018-1, 2014.

Sato, K. and Okamoto, H., Global Analysis of Height‐Resolved Ice Particle Categories From Spaceborne Lidar, Geophysical Research Letters, 50, https://doi.org/10.1029/2023gl105522, 2023.

Sato K., Okamoto H, Nishizawa T., Jin Y., Nakajima T., Wang M., Satoh M., Roh W., Ishimoto H., Kudo R., JAXA Level 2 cloud and precipitation microphysics retrievals based on EarthCARE CPR, ATLID and MSI, Atmos. Meas. Tech., submitted, 2024.

Sherriff-Tadano, S., Abe-Ouchi, A., Yoshimori, M., , Ohgaito, R., Vadsaria, T, Chan, W-L., Hotta, H., Kikuchi, M., Kodama, T., Oka, A., and Suzuki, K.: Southern Ocean Surface Temperatures and Cloud Biases in Climate Models Connected to the Representation of Glacial Deep Ocean Circulation, DOI: 10.1175/JCLI-D-22-0221.1 , J. Climate, 2023.

Tomita H, Satoh M.: **A new dynamical framework of nonhydrostatic global model using the icosahedral grid.** *Fluid Dyn Res* , **34:** 357–400, 2004.

Watanabe, M., Suzuki, T., O'ishi, R., Komuro, Y., Watanabe, S., Emori, S., et al.: Improved climate simulation by MIROC5: Mean states, variability, and climate sensitivity. *Journal of Climate*, **23**, 6312–6335. **https://doi.org/10.1175/2010JCLI3679.1, 2010.**

https://doi.org/10.5194/amt-2024-103
Preprint. Discussion started: 5 August 2024

Watanabe, M., Shiogama, H., Yoshimori, M. *et al.* Fast and slow timescales in the tropical low-cloud response to increasing CO_2 in two climate models. *Clim Dyn* **39**, 1627–1641 (2012). https://doi.org/10.1007/s00382-011-1178-y, 2012.

Winker, D. M., Hunt, W. H. and McGill, M. J.: Initial performance assessment of CALIOP, Geophys. Res. Lett., 34, L19803, doi:10.1029/ 2007GL030135, 2007

Winker D. M., Pelon J, Coakley JA, Ackerman SA, Charlson RJ, Colarco PR, Flamant P, Fu Q, Hoff RM, Kittaka C, Kubar TL, Le Treut H, Mccormick MP, Mégie G, Poole L, Powell K, Trepte C, Vaughan M. A. and Wielicki B.A.: The CALIPSO mission. Bull Am Meteorol Soc 91:1211–1230. https://doi.org/10.1175/2010BAMS3009.1, 2010.

Yoshida, R., Okamoto, H., Hagihara, Y., and Ishimoto, H.: Global analysis of cloud phase and ice crystal orientation from Cloud - Aerosol Lidar and Infrared Pathfinder Satellite Observation (CALIPSO) data using attenuated backscattering and depolarization ratio, J. Geophys. Res., 115, https://doi.org/10.1029/2009jd012334, 2010.

Zelinka, M. D., Myers, T. A., McCoy, D. T., Po-Chedley, S., Caldwell, P. M., Ceppi, P., et al.: Causes of higher climate sensitivity in CMIP6 models. Geophysical Research Letters, 47, e2019GL085782. https://doi.org/10.1029/2019GL085782, 2020.